Computational model for low cycle fatigue analysis of lattice materials: Incorporating theory of critical distance with elastoplastic homogenization

European Journal of Mechanics / A Solids 92 (2022) 104480

Contents lists available at ScienceDirect

European Journal of Mechanics / A Solids

journal homepage: www.elsevier.com/locate/ejmsol

Computational model for low cycle fatigue analysis of lattice materials: Incorporating theory of critical distance with elastoplastic homogenization

Danial Molavitabrizi [a], Anders Ekberg [b], S. Mahmoud Mousavi [a,*]

[a] Division of Applied Mechanics, Department of Materials Science and Engineering, Uppsala University, 751 03 Uppsala, Sweden
[b] Department of Mechanics and Maritime Sciences, Chalmers University of Technology, 412 96, Gothenburg, Sweden

ARTICLE INFO

Keywords:
Low cycle fatigue
Lattice materials
Theory of critical distance
Elastoplastic homogenization

ABSTRACT

A novel numerical framework for low cycle fatigue analysis of lattice materials is presented. The framework is based on computational elastoplastic homogenization equipped with the theory of critical distance to address the fatigue phenomenon. Explicit description of representative volume element and periodic boundary conditions are combined for computational efficiency and elimination of the boundary effects. The proposed method is generic and applicable to periodic micro-architectured materials. The method has been applied to 2-D auxetic and 3-D kelvin lattices. The classical Coffin-Manson and Morrow models are used to provide fatigue life predictions (strain-life curves). Predicted fatigue lives for the auxetic lattice are shown to provide good correspondence to experimentally found fatigue lives from the literature.

1. Introduction

The term "metamaterial" refers to lightweight, architectured materials with tailored properties. Lattice materials, as a well-known class of metamaterials, have potential application in a range of engineering products, e.g. biomedical implants (Zhao et al., 2016) and lightweight sandwich structures (Molavitabrizi and Laliberte, 2020). Lattice materials have periodic microarchitecture and exhibit interesting mechanical features like negative Poisson's ratio and high specific stiffness. The elastic behavior of these materials is well-investigated, e.g. (Molavitabrizi and Mousavi, 2020), (Deshpande et al., 2001), (Dong et al., 2019) (Gazzo et al., 2020), (Wang and McDowell, 2004), (Warren and Kraynik, 1997) and (Boutin et al., 2020), but this is not the case when plasticity is involved. Moreover, most studies in this field have mainly focused on quasi-static loading and there has been less attention on cyclic loading and fatigue analysis. However, fatigue characterization is a very crucial step towards industrial adoption of these materials, as it accounts for almost 90% of failures in engineering products.

Earlier studies on the fatigue behavior of lattice materials were mainly experimental, with the aim of obtaining the stress-life (*S–N* or Wohler) curve in high cycle regime, e.g. (Côté et al., 2007a) and (Côté et al., 2007b). However, investigation of fatigue behavior through experiments is very time-consuming and expensive. Thus, numerical simulations are required to employ broader fatigue analyses. Demiray et al. (2009) studied the high cycle fatigue (HCF) behavior of 3-D kelvin cell by using a micromechanical model with beam elements. Hedayati et al. (2016) numerically and experimentally studied the fatigue behavior of rhombic dodecahedron lattice. It turned out that the prediction obtained by this numerical study is not valid for high stress amplitudes. Khalil Abad et al. (Masoumi Khalil Abad et al., 2013) used continuum shell elements to computationally analyze the HCF behavior of 2-D square and hexagonal lattices. They used 3-D solid elements to improve the simulation accuracy, as Simone and Gibson (1998) reported that numerical models with beam elements cannot capture stress concentrations at lattice joints (nodes) and may therefore provide unrealistic fatigue life predictions.

A number of recent studies have tried to establish a relation between additive manufacturing processes and fatigue lives of lattice samples. These studies were mainly experimental and considered a wide range of additive-manufacturing-related parameters like radii variation and scatter in *S–N* curves for struts (Burret al., 2020), strut orientation, node fillet and unit-cell size (Dallago et al., 2021) as well as processing parameters like laser power (Ashouriet al., 2020). Other studies emphasized on the development of computational models using 3-D solid elements to enable the fatigue analysis of 3-D lattices. Peng et al. (2020) used a parametric computational approach to study the effect of lattice relative density and unit-cell topology on HCF. Refai et al. (2020) did an experimental and numerical study to characterize the multiaxial HCF

* Corresponding author.
E-mail address: mahmoud.mousavi@angstrom.uu.se (S.M. Mousavi).

https://doi.org/10.1016/j.euromechsol.2021.104480
Received 11 August 2021; Received in revised form 21 October 2021; Accepted 22 November 2021
Available online 24 November 2021

behavior of a wide range of lattice materials. Kolen et al. (Kolken et al., 2021) experimentally investigated the HCF behavior of auxetic lattices. Recently, Tomazincic et al. (Tomažinčič et al., 2020) and (Tomažinčič et al., 2019) studied the low cycle fatigue (LCF) behavior of three 2-D lattices.

It is observed that the fatigue-related research in lattice materials was mainly devoted to the high cycle regime, while there are only a few studies on LCF capabilities. The topic has received even far less attention in 3-D domain, despite its relevance in many of the potential real-world applications, e.g. the use of lattice materials as energy absorber, or as the core material in gas turbine blades. The current paper contributes to the field by introducing a novel numerical framework for LCF analysis of 2- and 3-D lattices, using the concept of elastoplastic homogenization along with the theory of critical distance (TCD). The use of homogenization theory and periodic boundary condition (PBC) considerably reduces the computational time and assures that the obtained material properties are not affected by the boundaries. Moreover, the complex geometry of lattice materials often leads to highly localized stressed/strained areas which complicate fatigue analysis. A TCD approach is used to address this issue.

The paper starts with the derivation of weak form equations and introduction of computational elastoplastic homogenization scheme for cellular media. Then, the TCD approach along with some remarks regarding its implementation on lattice material are discussed. Next, the proposed fatigue methodology is introduced in a structured framework. Following this, the model is numerically implemented on two sample topologies, i.e. a 2-D auxetic and a 3-D kelvin unit-cells, where the finite element method is applied for structural analysis, and an in-house code is developed for post-processing and fatigue analysis. Finally, LCF behavior of sample topologies are characterized by providing the fatigue life predictions for a range of load amplitudes.

2. Elastoplasticity of periodic micro-architectured materials

Lattice materials are a class of periodic cellular or so-called micro-architectured solids. In order to characterize their linear and nonlinear behavior, we start first (in section 2.1) with the derivation of the weak form equations for the most generic case, i.e. cellular materials with no prior assumption on material and/or deformation behavior. The generic weak form formulation is then used to derive the governing equations for linear elastic and elastoplastic material behavior.

Lattice materials are formed by periodic arrangement of unit-cells. It is possible to characterize their mechanical behavior by studying a single unit-cell, also referred to as a representative volume element (RVE), along with periodic boundary condition (PBC). This is computationally a very efficient approach which guarantees that material properties are not affected by the boundaries. In section 2.2, the linear and nonlinear weak form equations of cellular solids are numerically formulated for an RVE (unit-cell) using finite element method (FEM) and PBC. Finally, the equations for derivation of elastic and elastoplastic effective material properties (based on averaging theory) are reviewed.

The derivations in sections 2.1 and 2.2 are discussed in detail, since the formulation provided in this paper is different from some of the preceding works. Previous studies, e.g. (Masoumi Khalil Abad et al., 2013) and (Hollister and Kikuchi, 1992), have often employed the asymptotic method with separate treatment of microscale and macroscale displacements, i.e. equilibrium equations are written in microscale and the finite element problem is solved for microscopic displacements. The current approach reduces complexity by solving the problem directly for the whole displacement field, i.e. simultaneously considering both microscale and macroscale displacements. This results in a relatively different weak form equation and finite element formulation for an elastoplastic periodic cellular media, which has not been widely referred in the literature to the authors' knowledge.

2.1. Equilibrium equation

Under static equilibrium conditions and in the absence of body forces, the weak form of equilibrium equations for a continuum body Ω in spatial description appears as

$$\int_{\Omega} \sigma_{ij}\delta\varepsilon_{ij}\mathrm{d}v = \int_{\partial\Omega} t_i\delta u_i\mathrm{d}s \tag{1}$$

The above equation is presented in Einstein notation, where σ_{ji}, ε_{ij}, t_i and δu_i are stress field, strain field, traction (defined on boundary $\partial\Omega$) and virtual displacement, respectively.

It is assumed that the strain field of a periodic cellular media can be decomposed into macroscopic strain field ($\bar{\varepsilon}_{ij}$) and microscopic strain field or local fluctuation (ε^*_{ij}), i.e. $\varepsilon_{ij} = \bar{\varepsilon}_{ij} + \varepsilon^*_{ij}$. Thus, the above equilibrium equation is written as

$$\int_{\Omega} \sigma_{ij}\delta\left(\bar{\varepsilon}_{ij} + \varepsilon^*_{ij}\right)\mathrm{d}v = \int_{\partial\Omega} t_i\delta u_i\mathrm{d}s \tag{2}$$

Considering the Hill-Mandel Lemma, e.g. see (Yvonnet, 2019), we have

$$\int_{\Omega} \sigma_{ij}\delta\left(\varepsilon^*_{ij}\right)\mathrm{d}v = 0 \tag{3}$$

Under the stated assumptions, this is the most generic form of equilibrium equation for a cellular media (no prior assumption was made on deformation and/or material behavior). Any material and/or geometrical behaviors can be obtained based on this equation. Two cases are considered and derived in this paper – a linear elastic media and an elastoplastic media under small deformations.

For the linear elastic case, employing Hooke's law in equation (3) leads to

$$\int_{\Omega} C_{ijkl}\varepsilon_{kl}\delta\left(\varepsilon^*_{ij}\right)\mathrm{d}v = 0 \tag{4}$$

resulting in the equilibrium equation for an elastic material with small deformations.

Equation (3) can also include material nonlinearity, e.g. plasticity. To linearize the weak from, the stress is linearized using the 1st-order Taylor expansion.

$$\sigma_{ij(\varepsilon+\Delta\varepsilon)} = \sigma_{ij} + \Delta\sigma_{ij} = \sigma_{ij} + \frac{\partial\sigma_{ij}}{\partial\varepsilon_{kl}}\Delta\varepsilon_{kl} \tag{5}$$

With this, equation (3) follows as

$$\int_{\Omega} \left(\sigma_{ij} + \frac{\partial\sigma_{ij}}{\partial\varepsilon_{kl}}\Delta\varepsilon_{kl}\right)\delta\varepsilon^*_{ij}\mathrm{d}v = 0 \tag{6}$$

This equation describes the behavior of an elastoplastic periodic cellular material with small deformation. It is the governing equation for most of the analyses conducted in this paper due to its computational efficiency and sufficient accuracy. The only exception is a single large deformation analysis to identify the loading strains as described in detail in section 4 (specifically in Fig. 1).

Equations (4) and (6) are used to address elastic and elastoplastic problems, respectively. These equations can be numerically solved with FEM and the method of Lagrange multipliers, which is elaborated in the following section.

2.2. Computational elastoplastic homogenization

For computational homogenization, due to periodicity of the lattice material and the assumption of scale separation, we consider the domain Ω to be the RVE of the heterogenous material, i.e. the unit-cell of the

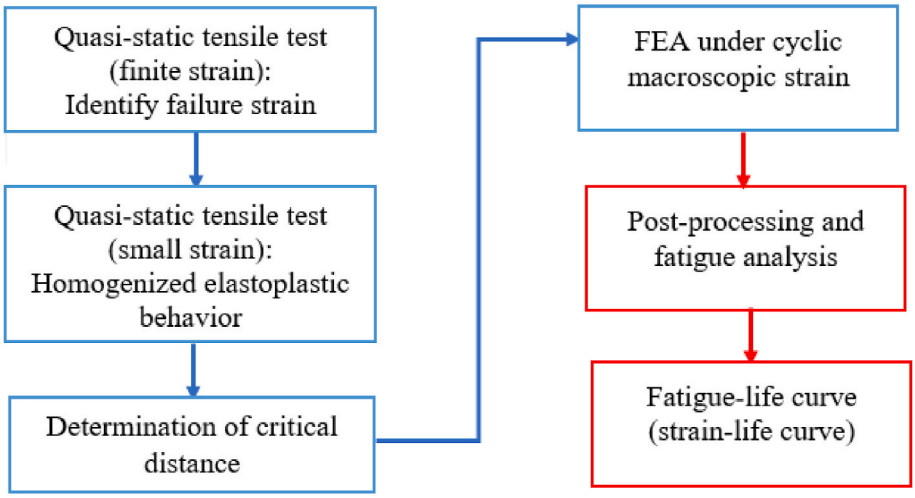

Fig. 1. Schematic of the proposed fatigue analysis model.

lattice. equation (6) depends not only on stress, σ_{ij}, but also on strain increments, $\Delta\varepsilon_{kl}$. Thus, an incremental-iterative approach is required to solve this equation. Since the equation is to be solved with FEM, the variables are now written in Voigt notation. Consequently, equation (5) is now written as

$$[\sigma^{n+1}] = [\sigma^n] + [\Delta\sigma] = [\sigma^n] + [D_{ep}][\Delta\varepsilon] \tag{7}$$

where $[D_{ep}]$ is the elastoplastic tangent matrix, as described in (Kim, (2015)). Superscripts n and $n+1$ denote the previous and current increments with $[\Delta\varepsilon] = [\varepsilon^{n+1}] - [\varepsilon^n]$. Following this, equation (6) becomes

$$\int_{\Omega} [\delta\varepsilon^*]^T \left([\sigma^n] + [D_{ep}][\Delta\varepsilon]\right) \mathrm{d}v = 0 \tag{8}$$

Using finite element formulation, the strain vector is defined as $[\varepsilon] = [B][u]$ and $[\Delta\varepsilon] = [B][\Delta u]$, where $[B]$ is the gradient of element shape function and $[u]$ is the element nodal displacements (includes both macro- and micro-scale, $[u^*]$, displacements). With this, equation (8) leads to

$$\int_{\Omega} [\delta u^*]^T \left([B]^T [D_{ep}][B]\right)[\Delta u] \mathrm{d}v = -\int_{\Omega} [\delta u^*]^T \left([B]^T [\sigma^n]\right) \mathrm{d}v \tag{9}$$

With $[\delta u^*]^T$ being the virtual microscopic displacement, we have

$$\int_{\Omega} \left([B]^T [D_{ep}][B]\right)[\Delta u] \mathrm{d}v = \int_{\Omega} \left(-[B]^T [\sigma^n]\right) \mathrm{d}v \tag{10}$$

The above equation is the linearized equilibrium equation for an elastoplastic cellular media which is to be discretized over an RVE and solved using PBC. The volume integral of the terms in parentheses on the left-hand side and right-hand side of the equation are, respectively, the element tangent stiffness matrix, $[k_t]$, and the element residual vector, $[res^n]$.

For a set of nodes being on two opposite sides of RVE, e.g. A and B, the periodicity condition is defined as $u_{(A)} - u_{(B)} = \bar{\varepsilon}(X_A - X_B)$, where X is the position of nodes (Yvonnet, 2019). This condition in the matrix form appears as

$$[P][U] = [R] \tag{11}$$

where, $[U]$ is the vector of unit-cell nodal deformations and matrix $[P]$ relates the deformation of paired nodes to the whole set of nodal deformations. For each set of paired nodes, $[R]$ is a column vector representing the right-hand side of periodicity condition. Additionally, a nodal displacement boundary condition is also required to prevent rigid body motion. Here, only constraining the translational degrees of a chosen node is sufficient, as rotational degrees of the unit-cell are automatically constrained by PBC. The method of Lagrange multipliers is employed to find the nodal displacements and reaction forces. The system of equations is formulated as

$$\begin{bmatrix} [K_t] & [P^T] & [Q^T] \\ [P] & [\varnothing] & [\varnothing] \\ [Q] & [\varnothing] & [\varnothing] \end{bmatrix} \begin{bmatrix} [\Delta U] \\ [\Delta\Lambda_1] \\ [\Delta\Lambda_2] \end{bmatrix} = \begin{bmatrix} [Res^n] \\ [\Delta R] \\ [\varnothing] \end{bmatrix} \tag{12}$$

where, $[K_t]$ is the assembled tangent stiffness matrix, $[Res^n]$ is the assembled residual vector and $[Q]$ constrains the translational degrees of a chosen node. Finally, $[\Delta\Lambda_1]$ and $[\Delta\Lambda_2]$ are the increments of Lagrange multipliers. These are required to update the reaction forces resulting from periodicity and rigid body constraints, respectively. Additionally, the problem is strain-controlled and therefore, in each increment we have a constant $[\Delta R] = [\Delta\bar{\varepsilon}][X_A - X_B]$.

The above system of equations is solved iteratively for strain increments using Newton–Raphson method, as described in (Kim, (2015)). In the case of elastic analysis, the problem becomes linear, the residual vector vanishes and there is no need for an incremental-iterative solver. Additionally, the assembled tangent stiffness matrix simplifies to classical global stiffness matrix, see (Molavitabrizi and Mousavi, 2020) and (Yvonnet, 2019) for details on elastic analysis.

Homogenization techniques are employed for mechanical characterization of heterogeneous materials. Among different techniques, the averaging method is one of the most suitable ones for derivation of quasi-static properties (Molavitabrizi and Mousavi, 2020). The method is established for both elastic and elastoplastic heterogeneous materials, see (Yvonnet, 2019) and (Gross and Seelig, 2018), but it is briefly reviewed here.

As was discussed in section 2.1, lattice materials are multiscale materials with microscopically fluctuating fields. The behavior of these materials can be characterized with their macroscale stress/strain fields. Consider a lattice RVE defined in region Ω of the space, subjected to a uniform macroscopic strain $\bar{\varepsilon}$ at the boundaries. Based on the averaging theory, the material macroscopic stress $\bar{\sigma}$ and strain can be obtained by taking the volume average of the stress and strain field over the RVE domain.

$$\begin{aligned} [\bar{\sigma}] &= <[\sigma]> = \frac{1}{V_{RVE}} \int_{\Omega} [\sigma_{(x)}] \mathrm{d}V \\ [\bar{\varepsilon}] &= <[\varepsilon]> = \frac{1}{V_{RVE}} \int_{\Omega} [\varepsilon_{(x)}] \mathrm{d}V \end{aligned} \tag{13}$$

Here, the volume averaging operator is denoted by <>. Now,

considering Hooke's law for the homogenized linear elastic continuum, we have

$$[\bar{\sigma}] = [\mathbb{C}][\bar{\varepsilon}] \tag{14}$$

where $[\mathbb{C}]$ is the effective elasticity matrix of the homogenized media. In the presence of plasticity and under assumption of small deformations, the macroscopic strain field is additively decomposed into elastic and plastic parts, i.e. $[\bar{\varepsilon}] = [\bar{\varepsilon^e}] + [\bar{\varepsilon^p}]$. Therefore

$$[\bar{\sigma}] = [\mathbb{C}][\bar{\varepsilon^e}] = [\mathbb{C}]([\bar{\varepsilon}] - [\bar{\varepsilon^p}]) \tag{15}$$

In the elastoplastic regime, the macroscopic elastic and plastic strains do not follow the ordinary volume average described in equation (13), i.e. $[\bar{\varepsilon^p}] \neq < [\varepsilon^p] >$ and $[\bar{\varepsilon^e}] \neq < [\varepsilon^e] >$. They are indeed the weighted average of their respective microscopic fields, e.g. see (Gross and Seelig, 2018). That is:

$$[\bar{\varepsilon^p}] = [\mathbb{C}]^{-1} < [\varepsilon^p]^T [C][M] >^T \tag{16}$$

where $[\varepsilon^p]$ is the elastic strain vector, $[C]$ is the elasticity tensor of the base material and $[M]$ is the localization matrix, i.e. $[B][u]$ in FEM implementation.

From the above equations, it is observed that the concept of homogenization is based on the equivalency of averaged microscopic stress/strain fields with their macroscopic counterparts. This means that the selected RVE (a single unit-cell for periodic materials) along with PBC represent the material's macroscopic behavior in terms of stress/strain levels. This equivalency assures that the RVE can accurately represent the fatigue life if the fatigue model is selected from stress- and/or strain-based approaches.

3. Theory of critical distance

Engineering components often possess geometrical features leading to localized stress/strain concentrations, and this challenges the fatigue-life prediction. One way to tackle this is to use a set of phenomenological methodologies known as theory of critical distance (TCD) (Taylor, 2010). TCD refers to a group of methods which use a critical domain for stress/strain assessment and fatigue analysis. The method is divided into four sub-classes: point method (PM), line method (LM), area method (AM) and volume method (VM) (Taylor, 2010). For the PM, the effective stress/strain is considered at a certain distance from the point of the stress/strain concentration. The effective stress/strain in LM, AM and VM is obtained, respectively, by averaging the stress/strain over a critical line, area, or volume defined around the point of stress/strain concentration. The averaged (or point value) of the stress/strain is considered representative for the fatigue behavior of the stress/strain concentration. The theory was initially proposed for HCF, see e.g. Taylor (2010), Neuber (1958) and Peterson (PETERSON et al., 1959), but recently, it has been successfully adopted for LCF as well, e.g. (Susmel and Taylor, 2010), (Faruq and Susmel, 2019), (Zhu et al., 2018) and (Pereira et al., 2020).

Lattice materials often have complex geometries which result in high stress/strain gradients and localized stress/strain concentrations. This makes their fatigue analysis challenging, and the challenge has been recognized in the literature, e.g. see (Refai et al., 2020) and (Lohmuller et al., 2018). To resolve the issue, the TCD is employed for the first time in this study to assess the LCF behavior of lattice materials. Among different TCD methods, the area method (AM) is selected as the most suitable method for this study. Although PM and LM are the most common and widely used models (due to the ease of implementation) (Taylor, 2010), they may not be suitable for the analysis of lattices, especially 3-D topologies. This is because lattice materials often show high stress/strain gradients in different spatial directions, and this makes the identification of critical distance by means of PM or LM a very tedious task. Moreover, it has been experimentally observed that in lattice materials, fatigue initiates from the surface of struts (in the vicinity of struts connections) (Boniotti et al., 2019). Therefore, the use of AM seems to be more reasonable as compared to VM.

In this work, the critical area is defined as the surface area resulting from the intersection of unit-cell surface with a circle (in 2-D) or a sphere (in 3-D) centered on the point of strain concentration. This definition is slightly different from what is typically considered as critical area, i.e. semicircle or hemisphere (see (Taylor, 2010) and (Pereira et al., 2020) for example), and the reason is that the classical definition is not applicable to the complex microarchitecture of lattice materials, especially for 3-D lattices. The schematic of the critical area and its practical implementation (especially for 3-D case) is more explained in section 5.3.

If the surface of the critical region (resulting from the intersection) is defined as $\partial\Omega_c$, the effective strain obtained via AM is formulated as

$$(\varepsilon_{ij})_{eff} = \frac{1}{A_c}\int_{\partial\Omega_c} \varepsilon_{ij}\,\mathrm{d}(\partial\Omega_c) \tag{17}$$

where A_c is the surface area of the critical region and ε_{ij} is the strain component of interest.

To consider multiaxial effects at lattice joints (nodes), the equivalent strain range is defined as (Pereira et al., 2020)

$$\Delta\varepsilon_{eq} = \frac{\sqrt{2}}{3} \times \sqrt{(\Delta\varepsilon_{11} - \Delta\varepsilon_{22})^2 + (\Delta\varepsilon_{22} - \Delta\varepsilon_{33})^2 + (\Delta\varepsilon_{33} - \Delta\varepsilon_{11})^2 + \frac{3}{2}(\Delta\varepsilon_{12}{}^2 + \Delta\varepsilon_{23}{}^2 + \Delta\varepsilon_{13}{}^2)} \tag{18}$$

where $\Delta\varepsilon_{ij}$ is the strain variation in each load cycle, that is $(\varepsilon_{ij})_{max} - (\varepsilon_{ij})_{min}$. Here, equation (18) is used for the calculation of both effective plastic strain range and effective total strain range. This equation is used after averaging the strain components on the critical area, as given in (17).

The obtained equivalent strain range is evaluated by two different fatigue prediction models, namely Coffin-Manson (COFFIN, 1954), (Manson, 1953) and Morrow (1965) (superposition of the models of Coffin-Manson and Basquin (BASQUIN, 1910)). The Coffin-Manson model only considers plastic strains, while Morrow's relation uses both elastic and plastic strains (total strain) for fatigue life prediction. The Coffin-Manson and Morrow relations, respectively, read as

$$\frac{\Delta\varepsilon_{eq}{}^p}{2} = \varepsilon_f'(2N)^c \tag{19-a}$$

$$\frac{\Delta\varepsilon_{eq}}{2} = \frac{\Delta\varepsilon_{eq}{}^e}{2} + \frac{\Delta\varepsilon_{eq}{}^p}{2} = \frac{\sigma_f'}{E}(2N)^b + \varepsilon_f'(2N)^c \tag{19-b}$$

where σ_f' is fatigue strength coefficient, b is fatigue strength exponent, ε_f' is fatigue ductility coefficient, c is fatigue ductility exponent and $2N$ is the number of stress/strain reversals before crack initiation (each cycle has two reversals).

4. Methodology outline

In this section, a new methodology is proposed for LCF analysis of

lattice materials, i.e. combination of TCD and elastoplastic homogenization. The methodology is outlined as following.

The method aims at the uniaxial LCF analysis of lattice materials. It is based on computational strain-controlled type of analysis, and thus, requires determination of loading strains. The loading strain can be obtained through a numerical analysis of a quasi-static uniaxial tensile test. This is made in a first step through a large deformation elastoplastic finite element analysis (FEA) on a lattice unit-cell featuring PBC. The large deformation analysis is employed to determine the macroscopic failure strain. Remaining analyses employ small deformation assumptions (to enhance the computational efficiency) unless stated otherwise. In the second step, a quasi-static small stain simulation is performed on the lattice RVE as described in section 2.2. Here, the maximum load (strain level) is set to be the failure strain obtained from the large strain simulation of the unit-cell. The macroscopic failure strain is then used for the estimation of the critical distance, see section 5.2 for more details. This distance is thus selected such that it can represent the macroscopic failure of the lattice material at the local (microscale) level. Once the critical distance has been identified, a set of elastoplastic simulations are run for various cyclic macroscopic strains. COMSOL Multiphysics® solvers are used for solid mechanics analyses. However, the results are imported into an in-house MATLAB code for post-processing and fatigue analysis, as discussed in section 3. The schematic of the method is demonstrated in Fig. 1, where blue and red colors distinguish COMSOL solvers from the MATLAB code in the design process.

Following the above-mentioned steps, the combined fatigue model is practically implemented on two sample lattice materials in the next section.

5. Numerical implementation and results

In this section, the step-by-step implementation of the proposed computational model (section 4) is demonstrated for a 2-D auxetic and 3-D kelvin unit-cell. The aluminum alloy 7075-T651 is selected as the base (bulk) material of the lattice samples. The static and fatigue properties of this alloy are reported in (Tomažinčič et al., (2019)), and are summarized in Table 1. The material shows kinematic hardening behavior (Tomažinčič et al., 2019), and thus, linear kinematic hardening is selected for the material model. To find the value for tangent modulus, a numerical tensile test is carried out on the test specimen, and results are calibrated with the experimental strain–stress curve provided in (Tomažinčič et al., (2019)). The details of the numerical test are not given here for brevity.

5.1. RVE topology

Recently, there has been a growing interest towards the application of auxetic lattices, e.g. (Kolken et al., 2021), (Tomažinčič et al., 2020), (Novak et al., 2021), (Mirzaali et al., 2020), (Lan et al., 2021), (Bonfanti and Bhaskar, 2018) and (Alkhader et al., 2020). The main feature of these materials is their negative Poisson's ratio at macroscale, i.e. their cross-sectional area expands under axial tension and shrinks under compression. This feature classifies such lattices as a so-called mechanical metamaterial. Hence, a 2-D auxetic is selected as the candidate material for LCF characterization. The schematic of the lattice sample and its RVE is presented in Fig. 2, where the RVE length in x and y directions are 11.4 mm and 22.1 mm, respectively. Also, the in-plane and out-of-plane thickness of struts are 1.7 mm and 2 mm, respectively. This lattice is simulated with plane-strain assumption. This is an established and valid assumption for plate lattices, as they are much stiffer in the out of plane direction (z-direction in this case).

Kelvin cell (also known as tetrakaidekahedron) is a space-filling unit-cell, which nearly satisfies the minimum surface energy and can reasonably represent the unit-cell of an open-cell foam (Zhu et al., 1997). Open-cell foams are used for high temperature applications, energy absorption as well as sound isolation, see e.g. (Belardi et al., 2021), (Zhu et al., 2017) and (Gao et al., 2017). Thus, this lattice is of great interest for the industry. The schematic of the space filling RVE and its macroscopic lattice sample is shown in Fig. 2. This form of RVE is suitable for the implementation of the described computational homogenization scheme, as the macroscopic kelvin lattice can be obtained by tessellation of the RVE along coordinate axes. The length of the cubic RVE is 12.7 mm and the radius of struts is 2.54 mm. The relative density of the lattice is 20.6%.

Before proceeding with the design methodology, the importance of homogenization and PBC in elimination of boundary effects is highlighted through a comparison between numerical and experimental tensile tests on an auxetic lattice sample. It is to be noted that 8-node rectangular (plane-strain) and 10-node tetrahedral elements are used for 2- and 3-D simulations, respectively. A fine mesh is used to ensure convergence in the analyses. The minimum element size in 2- and 3-D models being 0.02 mm and 0.05 mm, respectively.

5.2. Boundary effects

To characterize the tensile behavior of the lattice, a macroscopically strain controlled elastoplastic FEA with PBC is conducted on the unit-cell (RVE). The results are then homogenized, based on equation (13), to characterize the macroscopic behavior of the lattice. The obtained stress–strain curve is then compared with the experimental study carried out in (Tomažinčič et al., (2019)). The experimental sample used in (Tomažinčič et al., (2019)) has 9 unit-cells (3 unit-cells in each direction, i.e. 3×3 unit-cells). However, for mechanical characterization of lattice materials, it is very crucial to have a sample with an adequate number of unit-cells to avoid boundary effects. This can be numerically achieved with PBC, as it mimics the condition of an infinite number of unit-cells and guarantees that the results are not altered by boundaries. Comparing the results in Fig. 3 reveals that the number of unit-cells in the test specimen used in (Tomažinčič et al., (2019)) is not sufficient.

To validate this claim and assess the results obtained by PBC, a set of numerical experiments of tensile tests is conducted on samples with different number of unit-cells, where one end is clamped and the other end displaced in the x-direction, see Fig. 4. An elastoplastic FEA is performed and the middle unit-cell (with the largest distance from the boundaries) is isolated to assess the behavior of the lattice. Following the elastoplastic homogenization rules (section 2.3), the stresses are averaged over the RVE (isolated unit-cell), and the macroscopic behavior of the lattice is derived. The results of these numerical experiments (Fig. 3) show that as the number of unit-cells in a sample increases, its stress-strain curve converges towards the one obtained by PBC. Eventually, it turned out that a sample with at least 81 unit-cells (9 unit-cell in each direction, i.e. 9×9 unit-cells) can closely represent the behavior of an infinite lattice (single unit-cell with PBC).

Table 1
Properties of Al 7075-T651 alloy.

Static properties (Tomažinčič et al., 2019)				Hardening	Fatigue parameters (Tomažinčič et al., 2019)			
Young Modulus (GPa)	Yield strength (MPa)	Ultimate tensile strength (MPa)	Elongation to failure (%)	Tangent modulus (GPa)	$\sigma_f^{'}$ (MPa)	$\varepsilon_f^{'}$	c	b
68.9	539	596	10.5	0.4	114.5	0.0686	−0.3605	−0.0048

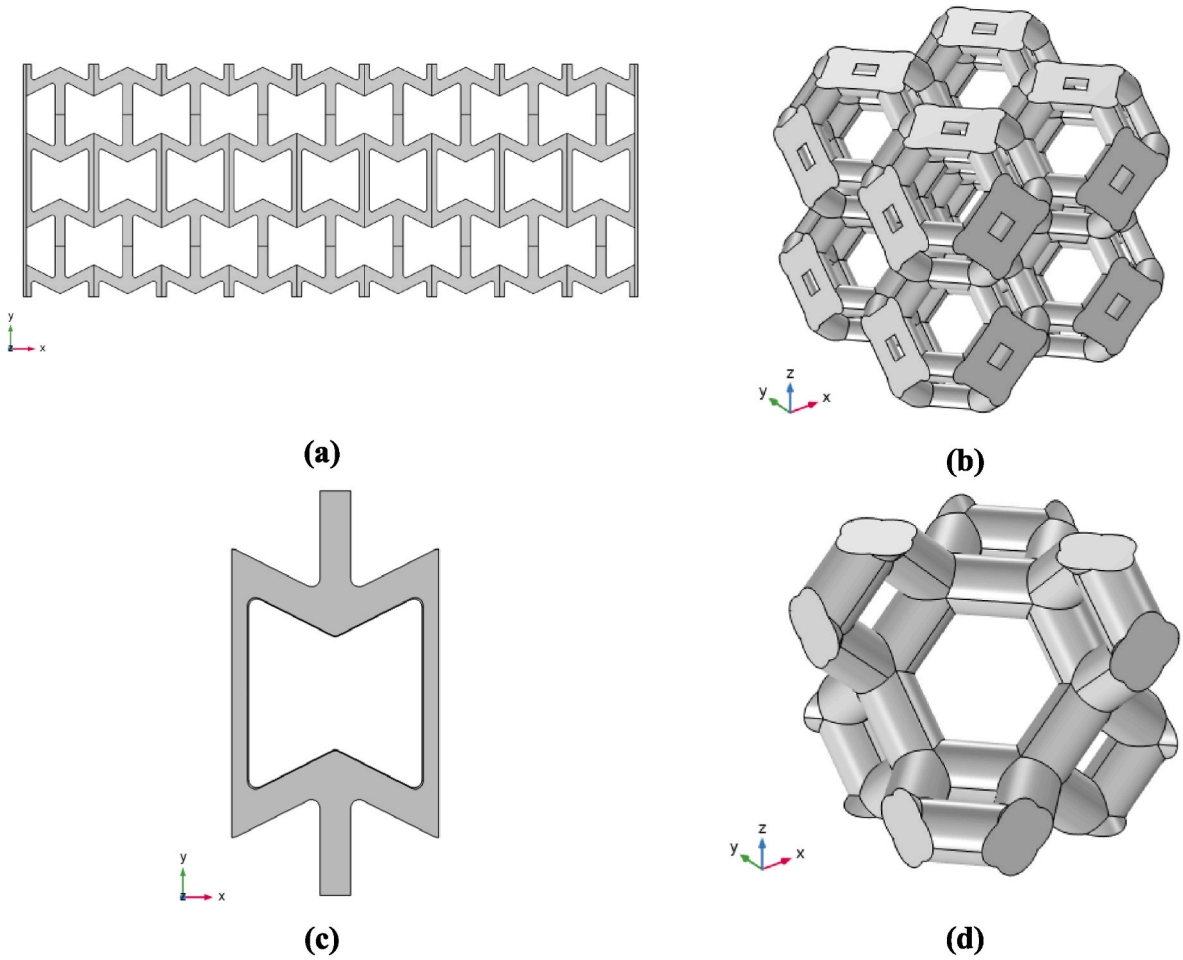

Fig. 2. Schematic of the lattice samples and their RVEs (unit-cells): (a) auxetic sample; (b) kelvin sample, (c) 2-D auxetic RVE, and (d) 3-D kelvin RVE.

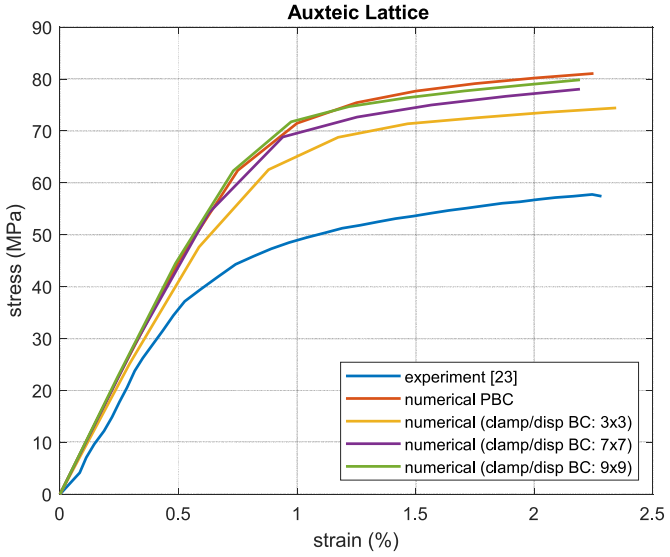

Fig. 3. Numerical vs experimental (Tomažinčič et al., 2019) stress-strain curves for the tensile test (*xx*-direction). Data for: experiment (with 3 × 3 unit-cells), numerical with clamp/disp. BC (with 3× 3 unit-cells), numerical with clamp/disp. BC (with 7× 7 unit-cells), numerical with clamp/disp. BC (with 9× 9 unit-cells) and numerical with PBC (with an infinite number of unit-cells enforced by PBC).

Additionally, manufacturing defects could possibly contribute to the discrepancies. For example, the sample in (Tomažinčič et al., (2019)) was manufactured using waterjet cutting process which produces noticeable surface roughness and influences the strain-stress state. Note however that the surface roughness typically has a minor effect on static behavior and/or the low cycle fatigue resistance.

The above simulations highlight the fact that under uniform loading conditions, e.g. uniaxial loading in this case, an RVE (single unit-cell) along with PBC can effectively represent the stress and/or strain field of a macroscopic lattice with a large number of unit-cells. Accordingly, the use of single unit-cell with PBC is suitable for stress- and/or strain-based uniaxial (or even multiaxial) fatigue analysis. In such cases, using a single unit-cell with PBC is computationally far more efficient compared to the simulation of a large arrangement of unit-cells with clamped/displaced BC.

5.3. Computational fatigue model

Now, the design methodology is elaborated step by step. The explained elastoplastic computational scheme (FEM/homogenization) in conjunction with the TCD approach are used as the main design strategies. Numerical tests are conducted under a uniaxial macroscopic strain ($\bar{\varepsilon}_{xx}$) loading condition, which under linear conditions leads to a proportional cyclic state of strain locally. In general, the plasticity may introduce some non-linearity but as can be seen in Fig. 10, its influence on proportionality is limited here. Hence, the equivalent strain method, equation (18), would still provide a good characterization of the fatigue impact.

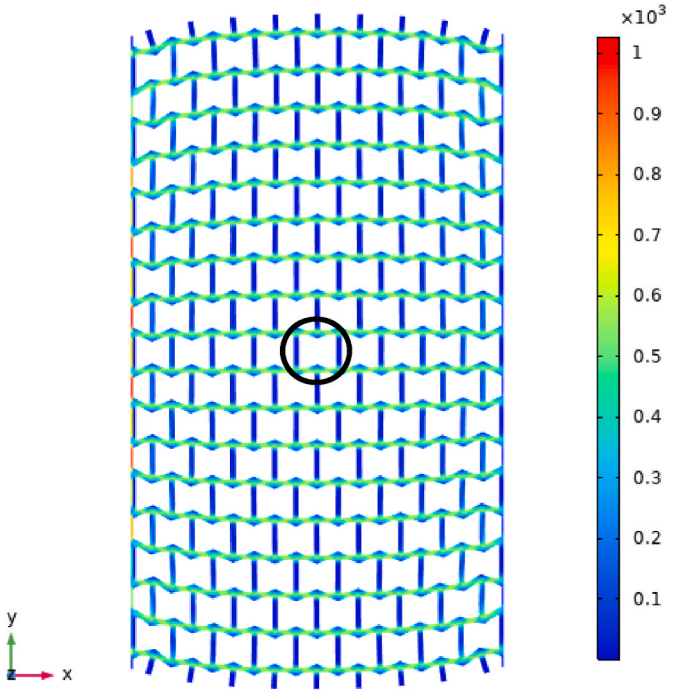

Fig. 4. Numerical analysis of a tensile test with clamped/displacement BC (von Mises stress distribution); left-side is clamped and right-side displaced in x-direction. The isolated unit-cell is marked with black circle.

5.3.1. *Large deformation*

The first step towards the LCF analysis of lattice materials is the identification of the macroscopic loading strain. This loading is considered to be in the range between the macroscopic yield and failure strain. However, the tensile behavior of lattice materials is not yet well-established and is an active field of research, see for example (Ronan et al., 2016), (Tankasala et al., 2017) and (Seiler et al., 2020) in which the topic is explored for a number of 2-D topologies. This is even more challenging and less established when it comes to 3-D samples. In fact, very few studies have experimentally and/or numerically investigated the topic. Therefore, we aim for the numerical characterization of tensile behavior of lattices using large deformation elastoplastic analysis. This is performed on a single unit-cell with PBC, and typical assumptions related to large deformation theory. It is of the interest to evaluate the field variables in reference configuration (material frame). Thus, using the results of FEA and following equation (13), the second Piola-Kirchhoff stress is averaged over the RVE volume in the reference configuration. This is plotted in Fig. 5. Here, failure is assumed to occur when the averaged (effective) second Piola-Kirchhoff stress starts to decrease. No material softening mechanism (damage) is included in the constitutive model, since this would require additional uncertain material data. Consequently, reduction of the averaged stress can be contributed to the structural softening caused by the plasticity. For the auxetic and kelvin cells this point, respectively, corresponds to the total strain of 5.75% and 4.5%. This is considered as the failure strain of the lattice and pointed out in Figs. 5 and 6.

The large deformation (finite strain) analysis is performed only to characterize the tensile behavior of the lattice. The failure strain determined in this analysis is the input to the following fatigue analysis which is carried out with the small deformation assumption.

5.3.2. *Elastoplastic FEA/Homogenization*

A macroscopically strain-controlled ($\bar{\varepsilon}_{xx}$) elastoplastic analysis with PBC is conducted on the lattice RVE. The total macroscopic strain, $\bar{\varepsilon}_{xx}$, is incrementally increased from zero up to the failure point, and the finite element problem, equation (12), is solved at every load increment. Then, using the data obtained from FEA, the elastoplastic homogenization scheme (section 2.2) is implemented, and stresses are averaged over the RVE (unit-cell). The average stress-strain relationship characterizes the macroscopic behavior of the lattice, as shown in Figs. 7 and 8.

Investigating the results provided in Figs. 7 and 8, the macroscopic yield strains of auxetic and kelvin cells are found to be 0.75% and 1%, respectively. These points were selected when the slope of the macroscopic stress-strain curve has deviated from linear elastic behavior. In this study, this strain level is taken as the lower bound for LCF analyses.

5.3.3. *Determination of critical distance*

From FEA, it is observed that the lattices fail locally at unit-cell joints (corners), i.e. local stresses exceed the base material's yield strength, well before the occurrence of macroscopic yielding, i.e. well before 0.75% strain in auxetic and 1% strain in kelvin. This indicates that any fatigue/failure assessment based on the critical element/node (highly strained elements/nodes at joints) would lead to unrealistic results. Hence, following the theory of critical distance, the aim is to find a

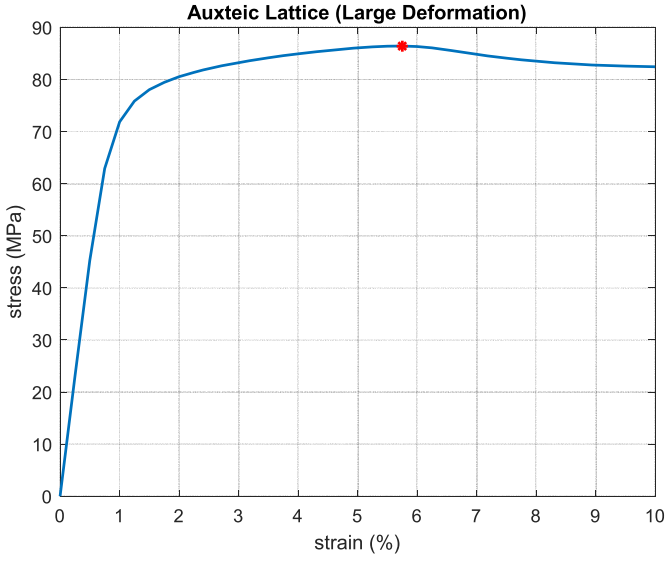

Fig. 5. Auxetic lattice: averaged Piola-Kirchhoff stress (*xx*-direction) vs macroscopic strain.

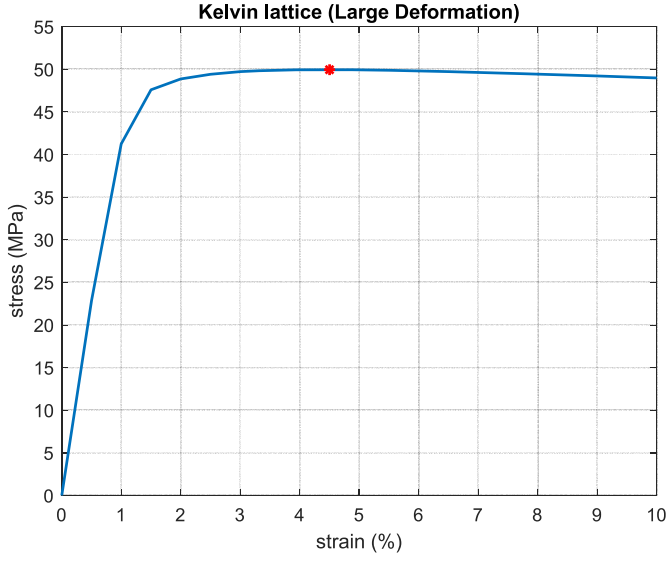

Fig. 6. Kelvin lattice: averaged Piola-Kirchhoff stress (*xx*-direction) vs macroscopic strain.

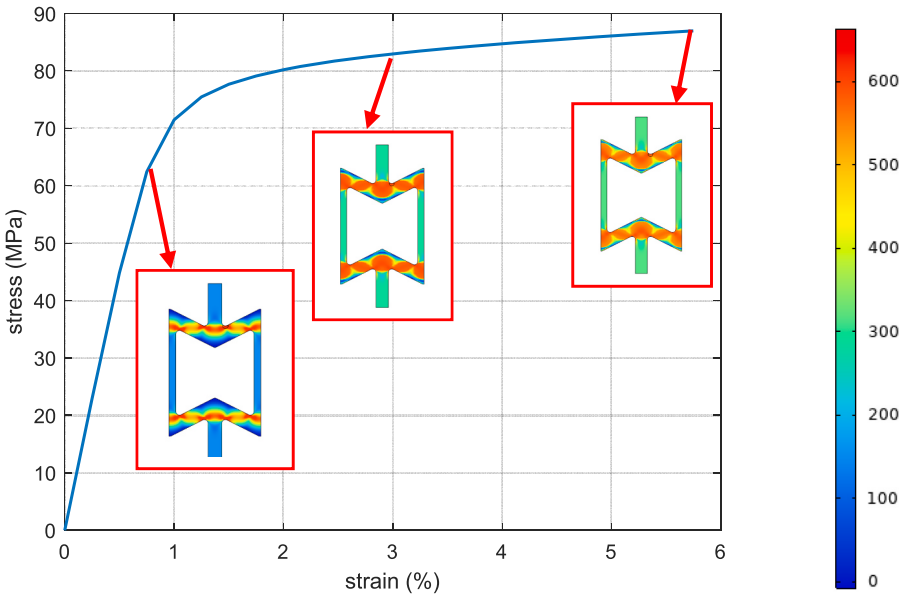

Fig. 7. Macroscopic stress-strain curve for auxetic lattice (*xx*-direction).

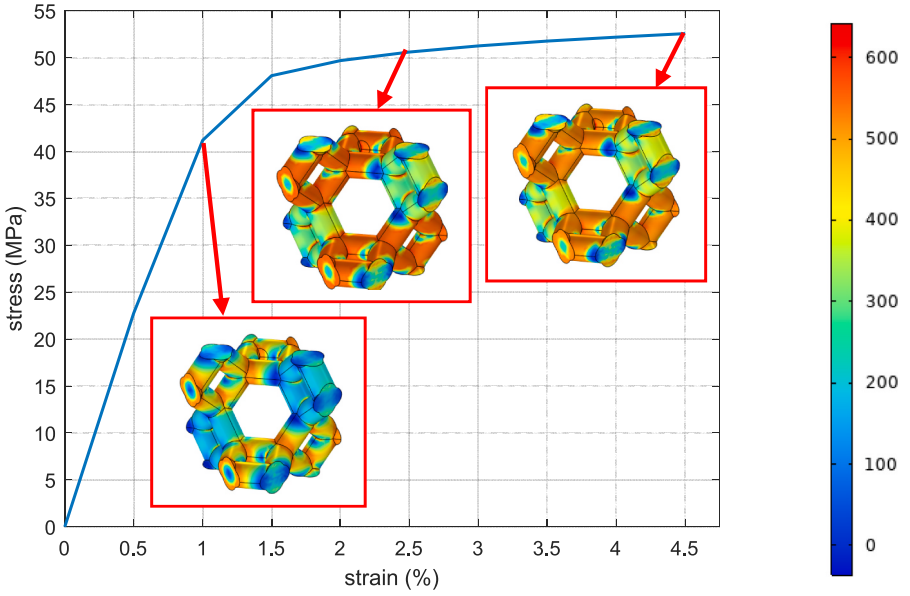

Fig. 8. Macroscopic stress-strain curve for kelvin lattice (*xx*-direction).

region around the strain/stress concentration, which can realistically represent the macroscopic behavior of the lattice. Ideally, this region should be evaluated based on the outcome of a (large) number of fatigue tests, e.g. see (Zhu et al., 2018). However, in the current study (and often in practice) there are no fatigue data for the material available. Under these circumstances we employ the fact that LCF is strongly correlated to plastic deformation. Hence, we define the critical area so that it reflects the plastic deformation characteristics of the structure. In other words, the plastic strain average over the selected region should reasonably demonstrate the macroscopic tensile behavior of the lattice. More specifically, when the macroscopic strain reaches the estimated failure point (5.75% strain in auxetic and 4.5% strain in kelvin), the average of plastic strain of the material in this region should correspond to the plastic failure strain of the base material, i.e. 9.7% plastic strain (plastic strain of Al-7075 at the point of softening). To sum up, the critical distance is determined such that the relation $(\varepsilon_{p,\text{avg}})_{lattice} \cong (\varepsilon_{p,\text{fail}})_{Al-7075} \cong 9.7$ % is stratified at the macroscopic failure load (strain). Here, ε_p is the plastic strain, and the subscript "lattice" represents the critical area on the lattice unit-cell (not the whole unit-cell).

It should be noted that the (quasi-static) failure strain can be considered as an extreme case of low-cycle fatigue with a fatigue life of one cycle. The use of such an extreme to establish the critical distance in LCF is analogous to the use of the fatigue limit (infinite fatigue life) to establish the critical distance in HCF analysis, see e.g. (Taylor, 2010).

As explained in section 3, the critical area is defined as the surface area resulting from the intersection of lattice unit-cell with a circle (in 2-D) or a sphere (in 3-D) centered on the point of the strain concentration. The concept of surface area in 2-D is intuitive but this may not be the case for 3-D lattices. In the tridimensional case, the surface area is the area formed by intersecting a volume (sphere centered on the point of strain concentration) with a surface of the lattice struts. In fact, what is highlight in Fig. 9-b is a surface (with no depth). It is to be reminded that

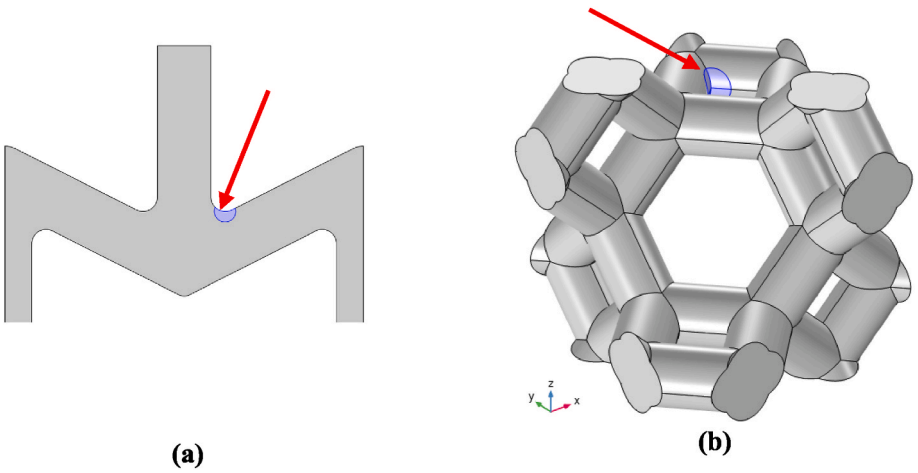

Fig. 9. The critical surface obtained on (a) RVE of auxetic lattice, and (b) RVE of kelvin lattice. The critical surface is highlighted in purple. (For interpretation of the references to color in this figure legend, the reader is referred to the Web version of this article.)

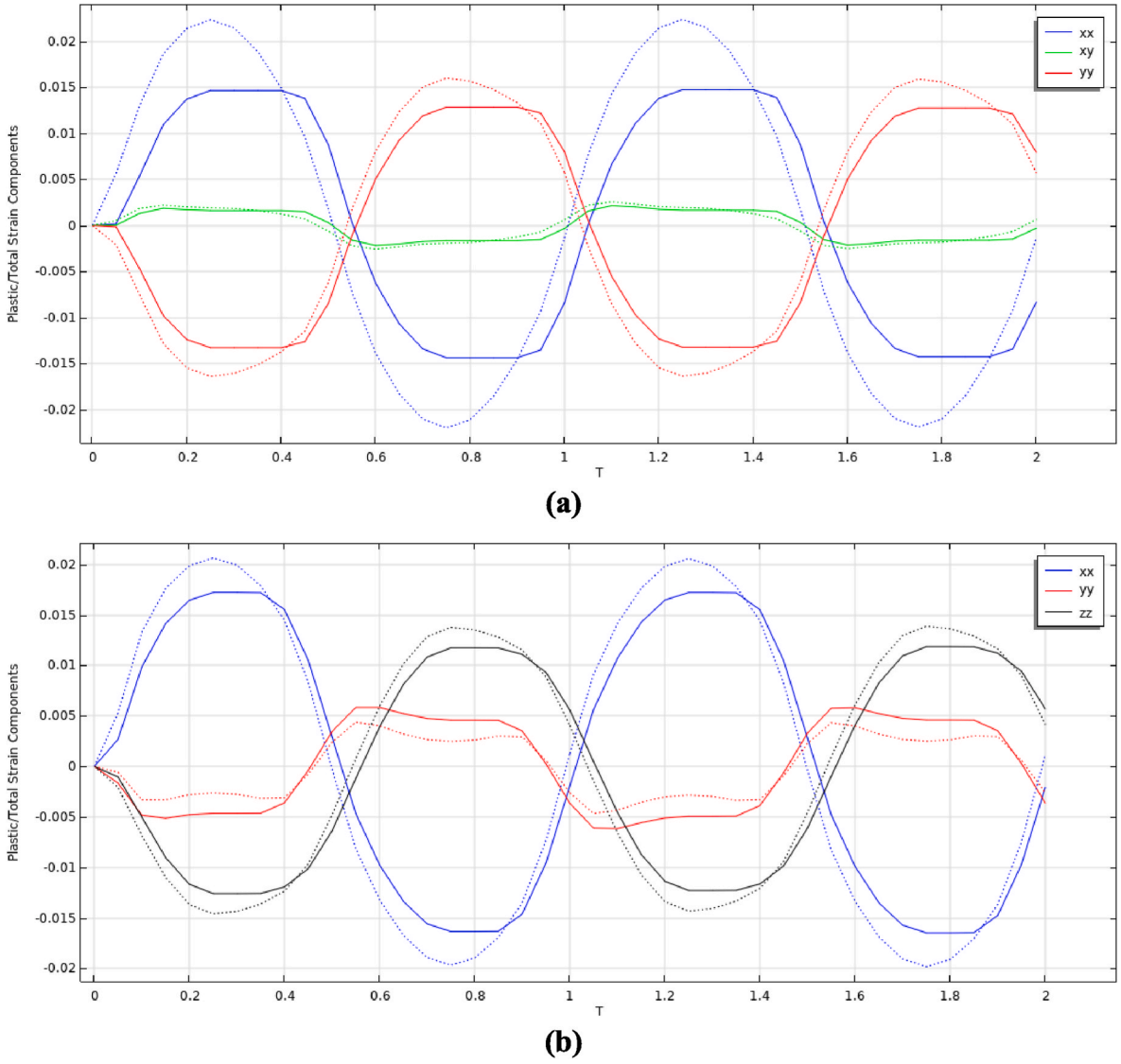

Fig. 10. Plastic/total strain components resulting from macroscopic cyclic loading: (a) auxetic with $\varepsilon_a = 1.25\%$, and (b) kelvin with $\varepsilon_a = 2\%$. The dotted and solid graphs represent total and plastic strains, respectively.

the AM is chosen over VM, since experimental observations (see e.g. (Boniotti et al., 2019)) show that fatigue in lattice predominantly initiates from the surface (in the vicinity of joints).

Following the above strategy for definition of the critical length, the radius of such circle for 2-D auxetic is obtained as 0.34 mm. For 3-D kelvin cell, this would be the radius of a sphere and is obtained as 1.38 mm. The critical surface (surface obtained from the intersection of unit-cell surface with defined circle/sphere) is demonstrated in Fig. 9.

5.3.4. Cyclic Loading & fatigue analysis

Once the lattice yield strain, failure strain and critical length (radius) is established, one can proceed with the fatigue analysis. Various strain amplitudes are considered, starting from the lattice yield strain. For fatigue analysis of the 3D model, a refined mesh with a minimum element size of 0.002 mm is used on the ciritical surface. Homogenization along with the application of PBC provides the possibility of employing such fine mesh resolution with reasonable computational costs. The fatigue assessment is carried out as below.

First, a cyclic macroscopic strain is defined, e.g. $\bar{\varepsilon}_{xx} = \varepsilon_a.\sin(2\pi T)$, where ε_a is the macroscopic strain amplitude and T is time, $T \in [n-1, n]$ with n being the load cycle number. The loading is macroscopically uniaxial and alternating (zero mean-stress). Under this loading condition, the elastoplastic FEA is conducted on the lattice RVE, following equation (12) in section 2.2 with a linear kinematic hardening material model. No averaging is involved at this first stage. Second, the plastic/total strain data obtained from FEA is averaged over the critcal surface, as given in (17). In lattice materials, the uniaxial macroscopic strain, $\bar{\varepsilon}_{xx}$, often results in a multiaxial total/plastic state of strain, especially at unit-cell joints (corners). For that reason, the equivalent total/plastic strain is obtained from the averaged total/plastic strain variation (over the critcal surface) using equation (18). Finally, this equivalent strain is used as an input for Coffin-Manson and Morrow models in equation (19), to calculate the fatigue life. An in-house MATLAB code, which takes the data obtained from the structural analysis as input is developed for this purpose.

As an example, the variation of the averaged total and plastic strains over the critical surface is demonstrated for the auxetic cell with $\varepsilon_a = 1.25\%$, and for the kelvin cell with $\varepsilon_a = 2\%$, see Fig. 10. The figure represents the data for the first and second load cycles depicting a very slight kinematic hardening effect. The fatigue analysis is done using data from the second load cycle, which is considered to represent the stabilized (plastic shake down) behavior.

Following the final step in the methodology, the fatigue life of auxetic and kelvin lattices are characterized for a range of strain amplitudes using both Morrow and Coffin-Manson models. The results are summarized in Tables 2 and 3, and the corresponding strain-life curves are visualized in semi-log plots in Figs. 11 and 12. Additionally, the numerical fatigue lives obtained for the auxetic lattice are compared with the experimental data provided in (Tomažinčič et al., (2019)), see Table 2 and Fig. 11. The results show a close match between numerical and experimental fatigue data. Note that the experimental fatigue lives are related to a finite lattice (see section 5.2) and comparing these to numerically evaluated lives of the infinite lattice implies an assumption

Table 2
Fatigue life estimates for low cycle regime (auxetic lattice).

Strain amplitude (ε_a)	N_i (Coffin-Manson)	N_i (Morrow)	N_i (Experiment (Tomažinčič et al., 2019))
0.0075	1733.8	398	No data
0.01	310.72	131.6	240
0.0125	128.30	68.20	90
0.015	65.75	39.9	38
0.02	26.40	18.40	No data
0.0325 ([a] 0.03)	5.94	4.90	3–24

[a] Refers to the applied experimental strain amplitude that is slightly different from the numerical one in the last row.

Table 3
Fatigue life estimates for low cycle regime (kelvin lattice).

Strain amplitude (ε_a)	N_i (Coffin-Manson)	N_i (Morrow)
0.01	5797.9	3547.3
0.015	1022.8	585.7
0.02	379.12	229.8
0.025	180.78	118.7
0.03	98.05	69.8

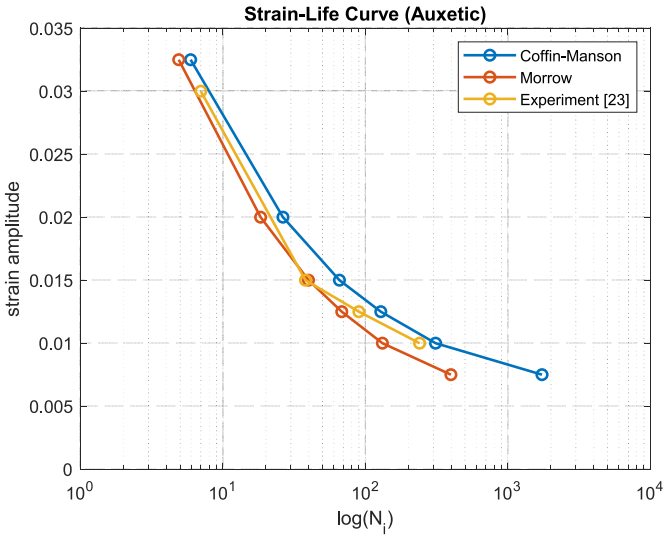

Fig. 11. Numerical and experimental (Tomažinčič et al., 2019) strain-life curve for LCF analysis of the auxetic lattice.

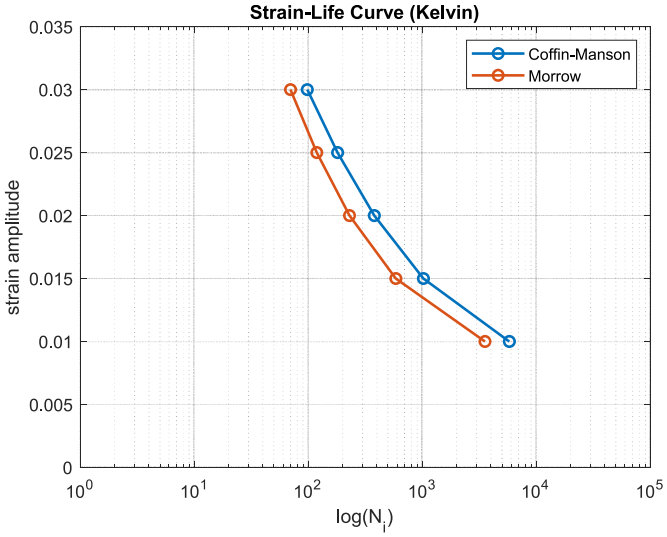

Fig. 12. Strain-life curve for LCF analysis of the kelvin lattice.

that the number of unit-cells (boundary effect) has a limited influence on LCF behavior. Finally, it can be noted that the difference in Coffin-Manson and Morrow curves is essentially due to the contribution of the elastic strains and the HCF part.

6. Conclusion

The LCF behavior of lattice materials is less-established, especially for 3-D topologies. The current paper proposed a novel fatigue methodology for the LCF analysis of both 2- and 3-D lattice materials. Due to

the general lack of available data on LCF and tensile behavior of lattice materials, this study was focused on providing a novel methodology for LCF analysis of lattices based on computational homogenization and the theory of critical distance. The input for the analysis is restricted to yield and LCF data from the base material. Numerical simulations featuring elastoplastic homogenization theory have been adopted to establish the yield point and failure strain of the lattice. These are then employed to derive the critical distance in the TCD approach for fatigue evaluation. The obtained data are then employed in LCF life predictions for lattice unit-cells, where periodic boundary conditions have been used to minimize computational demands. Following this methodology, two sample lattice topologies, namely auxetic and kelvin, were numerically tested and their corresponding strain-lives were characterized. Fatigue life predictions for the auxetic lattice show good correspondence to experimentally found fatigue lives reported in the literature.

This is the first work of its kind aiming at the investigation of LCF and tensile behavior of 2- and 3-D lattice materials from limited knowledge on fatigue characteristics of the lattice base material. The numerical framework presented in this study is generic and applicable to other lattice topologies or periodic micro-architectured materials, e.g. surface-based lattices. Of course, the fatigue criterion (Morrow in the current study) and the constitutive modeling should be adopted accordingly with regards to the base material. The proposed numerical model and the obtained results are to be further validated and calibrated in future experimental studies. In particular, the TCD method can benefit from further experimental results to quantify the accuracy of the approach.

Declaration of competing interest

The authors declare that they have no known competing financial interests or personal relationships that could have appeared to influence the work reported in this paper.

Acknowledgment

Danial Molavitabrizi and Mahmoud Mousavi acknowledge the financial support by the Starting Grant (2018-03636) from the Swedish Research Council (Vetenskapsrådet). Anders Ekberg's involvement is part of the ongoing activities in CHARMEC – Chalmers Railway Mechanics (www.chalmers.se/charmec). Part of his works has been funded from the European Union's Horizon 2020 research and innovation programme in the project In2Track3 under grant agreement No 101012456.

Appendix A. Schematic of applied PBC

The applied PBC on auxetic and kelvin cells are schematically illustrated in Figs. A-1 and A-2, respectively. Since the opposite boundaries of the 3-D Kelvin cell are not visible in a 2-D figure, their positions are highlighted with red arrows.

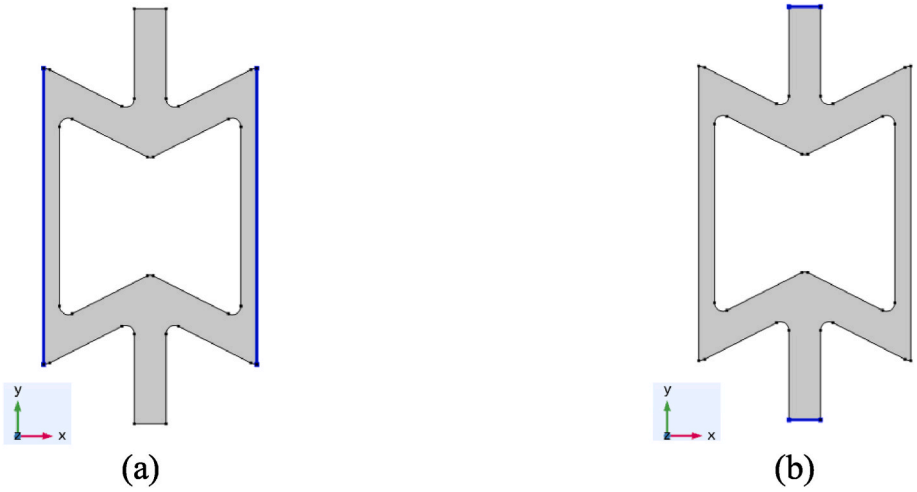

Fig. A-1. Schematic of the applied PBC on auxetic unit-cell; (a) periodicity in x-direction, and (b) periodicity in y-direction. (The constrained boundaries are highlighted in blue.)

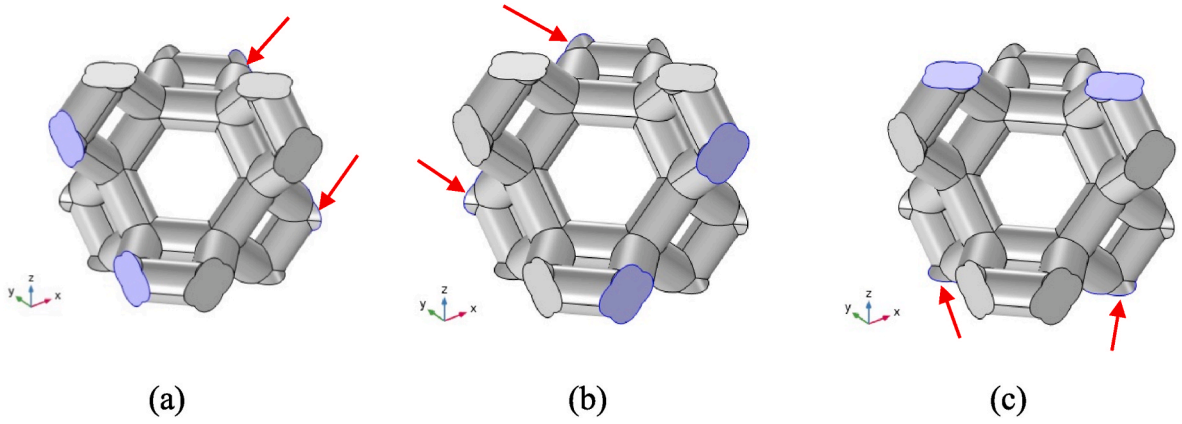

Fig. A-2. Schematic of the applied PBC on Kelvin unit-cell; (a) periodicity in x-direction, (b) periodicity in y-direction, and (c) periodicity in z-direction. (The constrained boundaries are highlighted in purple).

Appendix B. Schematic of critical area in TCD assessment

The critical area is defined as the surface area resulting from the intersection of lattice unit-cell with a circle (in 2-D) or a sphere (in 3-D) centered on the point of the strain concentration. This is schematically shown in Fig. B-1 for both 2-D auxetic and 3-D Kelvin cells. The defined circle (in 2-D) and sphere (for 3-D) are highlighted in purple and marked with red arrows. The intersection of these geometries with unit-cells forms the critical area.

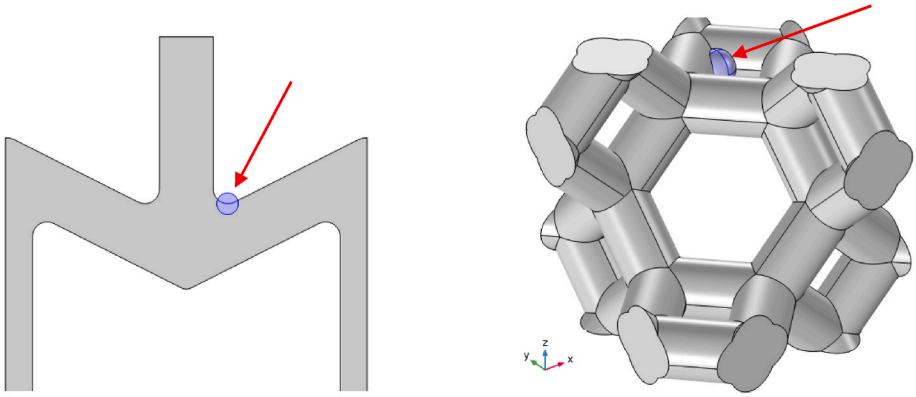

Fig. B-1. Schematic of how critical area is formed in the selected unit-cells.

References

Alkhader, M., Abuzaid, W., Elyoussef, M., Al-Adaileh, S., Mar. 2020. Localized strain fields in honeycomb materials with convex and concaved cells. Eur. J. Mech. Solid. 80, 103890. https://doi.org/10.1016/j.euromechsol.2019.103890.

Ashouri, D., et al., May 2020. Mechanical behaviour of additive manufactured 316L f2ccz lattice structure under static and cyclic loading. Int. J. Fatig. 134, 105503. https://doi.org/10.1016/j.ijfatigue.2020.105503.

Basquin, O., 1910. The exponential law of endurance tests. Proc Am Soc Test Mater 10, 625–630.

Belardi, V.G., Fanelli, P., Trupiano, S., Vivio, F., Aug. 2021. Multiscale analysis and mechanical characterization of open-cell foams by simplified FE modeling. Eur. J. Mech. Solid. 89, 104291. https://doi.org/10.1016/j.euromechsol.2021.104291.

Bonfanti, A., Bhaskar, A., Sep. 2018. Elastoplastic response and recoil of honeycomb lattices. Eur. J. Mech. Solid. 71, 77–88. https://doi.org/10.1016/j.euromechsol.2017.12.003.

Boniotti, L., Beretta, S., Patriarca, L., Rigoni, L., Foletti, S., Nov. 2019. Experimental and numerical investigation on compressive fatigue strength of lattice structures of AlSi7Mg manufactured by SLM. Int. J. Fatig. 128, 105181. https://doi.org/10.1016/j.ijfatigue.2019.06.041.

Boutin, C., Fossat, P., Droz, C., Ichchou, M., Jan. 2020. Dynamics of ribbed plates with inner resonance: analytical homogenized models and experimental validation. Eur. J. Mech. Solid. 79, 103838. https://doi.org/10.1016/j.euromechsol.2019.103838.

Burr, A., et al., Oct. 2020. A numerical framework to predict the fatigue life of lattice structures built by additive manufacturing. Int. J. Fatig. 139, 105769. https://doi.org/10.1016/j.ijfatigue.2020.105769.

Coffin Jr., L.F., 1954. A Study of the Effects of Cyclic Thermal Stresses on a Ductile Metal, vol. 76. Transactions of the American Society of Mechanical Engineers, New York, pp. 931–950.

Côté, F., Deshpande, V.S., Fleck, N.A., Apr. 2007. Shear fatigue strength of a prismatic diamond sandwich core. Scripta Mater. 56 (7), 585–588. https://doi.org/10.1016/j.scriptamat.2006.12.035.

Côté, F., Fleck, N.A., Deshpande, V.S., Aug. 2007. Fatigue performance of sandwich beams with a pyramidal core. Int. J. Fatig. 29 (8), 1402–1412. https://doi.org/10.1016/j.ijfatigue.2006.11.013.

Dallago, M., Raghavendra, S., Luchin, V., Zappini, G., Pasini, D., Benedetti, M., Jan. 2021. The role of node fillet, unit-cell size and strut orientation on the fatigue strength of Ti-6Al-4V lattice materials additively manufactured via laser powder bed fusion. Int. J. Fatig. 142, 105946. https://doi.org/10.1016/j.ijfatigue.2020.105946.

Demiray, S., Becker, W., Hohe, J., Mar. 2009. Investigation of the fatigue behavior of open cell foams by a micromechanical 3-D model. Mater. Sci. Eng., A 504 (1), 141–149. https://doi.org/10.1016/j.msea.2008.10.036.

Deshpande, V., Fleck, N.A., Ashby, M.F., Aug. 2001. Effective properties of the octet-truss lattice material. J. Mech. Phys. Solid. https://doi.org/10.1016/S0022-5096(01)00010-2.

Dong, G., Tang, Y., Zhao, Y.F., Jan. 2019. A 149 line homogenization code for three-dimensional cellular materials written in matlab. J. Eng. Mater. Technol. 141 (1) https://doi.org/10.1115/1.4040555.

Faruq, N.Z., Susmel, L., 2019. Proportional/nonproportional constant/variable amplitude multiaxial notch fatigue: cyclic plasticity, non-zero mean stresses, and critical distance/plane. Fatig. Fract. Eng. Mater. Struct. 42 (9), 1849–1873. https://doi.org/10.1111/ffe.13036.

Gao, K., van Dommelen, J.A.W., Geers, M.G.D., . Investigation of the effects of the microstructure on the sound absorption performance of polymer foams using a computational homogenization approach. Eur. J. Mech. Solid. 61, 330–344. https://doi.org/10.1016/j.euromechsol.2016.10.011.

Gazzo, S., Cuomo, M., Boutin, C., Contrafatto, L., Jul. 2020. Directional properties of fibre network materials evaluated by means of discrete homogenization. Eur. J. Mech. Solid. 82, 104009. https://doi.org/10.1016/j.euromechsol.2020.104009.

Gross, D., Seelig, T., 2018. Fracture Mechanics: with an Introduction to Micromechanics, third ed. Springer International Publishing. https://doi.org/10.1007/978-3-319-71090-7.

Hedayati, R., Hosseini-Toudeshky, H., Sadighi, M., Mohammadi-Aghdam, M., Zadpoor, A.A., Mar. 2016. Computational prediction of the fatigue behavior of additively manufactured porous metallic biomaterials. Int. J. Fatig. 84, 67–79. https://doi.org/10.1016/j.ijfatigue.2015.11.017.

Hollister, S.J., Kikuchi, N., Mar. 1992. A comparison of homogenization and standard mechanics analyses for periodic porous composites. Comput. Mech. 10 (2), 73–95. https://doi.org/10.1007/BF00369853.

Kim, N.-H., 2015. Introduction to Nonlinear Finite Element Analysis. Springer US. https://doi.org/10.1007/978-1-4419-1746-1.

Kolken, H.M.A., Garcia, A.F., Du Plessis, A., Rans, C., Mirzaali, M.J., Zadpoor, A.A., 2021. Fatigue performance of auxetic meta-biomaterials. *Acta Biomaterialia*, Mar. https://doi.org/10.1016/j.actbio.2021.03.015.

Lan, X., Meng, L., Zhao, J., Wang, Z., Nov. 2021. Mechanical properties and damage characterizations of 3D double-arrowhead auxetic structure with high-relative-density realized via selective laser melting. Eur. J. Mech. Solid. 90, 104386. https://doi.org/10.1016/j.euromechsol.2021.104386.

Lohmuller, P., Favre, J., Piotrowski, B., Kenzari, S., Laheurte, P., Jul. 2018. Stress concentration and mechanical strength of cubic lattice architectures. Materials 11 (7). https://doi.org/10.3390/ma11071146. Art. no. 7.

Manson, S.S., 1953. Behavior of Materials under Conditions of Thermal Stress. National Advisory Committee for Aeronautics.

Masoumi Khalil Abad, E., Arabnejad Khanoki, S., Pasini, D., Feb. 2013. Fatigue design of lattice materials via computational mechanics: application to lattices with smooth transitions in cell geometry. Int. J. Fatig. 47, 126–136. https://doi.org/10.1016/j.ijfatigue.2012.08.003.

Mirzaali, M.J., Pahlavani, H., Yarali, E., Zadpoor, A.A., Jul. 2020. Non-affinity in multi-material mechanical metamaterials. Sci. Rep. 10 (1) https://doi.org/10.1038/s41598-020-67984-6. Art. no. 1.

Molavitabrizi, D., Laliberte, J., Apr. 2020. Methodology for multiscale design and optimization of lattice core sandwich structures for lightweight hopper railcars. In: Proceedings of the Institution of Mechanical Engineers, Part C: Journal of Mechanical Engineering Science. https://doi.org/10.1177/0954406220920694, p. 0954406220920694.

Molavitabrizi, D., Mousavi, S.M., Nov. 2020. Elasticity of anisotropic low-density lattice materials. J. Eng. Mater. Technol. 143 https://doi.org/10.1115/1.4048931, 21007.

Morrow, J., Jan. 1965. Cyclic Plastic Strain Energy and Fatigue of Metals. Internal Friction, Damping, and Cyclic Plasticity. https://doi.org/10.1520/STP43764S.

Neuber, Heinz, 1958. Theory of Notch Stresses: Principles for Exact Calculation of Strength with Reference to Structural Form and Material, second ed. Springer Verlag, Berlin.

Novak, N., Duncan, O., Allen, T., Alderson, A., Vesenjak, M., Ren, Z., Jun. 2021. Shear modulus of conventional and auxetic open-cell foam. Mech. Mater. 157, 103818. https://doi.org/10.1016/j.mechmat.2021.103818.

Peng, C., Tran, P., Nguyen-Xuan, H., Ferreira, A.J.M., Mar. 2020. Mechanical performance and fatigue life prediction of lattice structures: parametric computational approach. Compos. Struct. 235, 111821. https://doi.org/10.1016/j.compstruct.2019.111821.

Pereira, J.C.R., de Jesus, A.M.P., Xavier, J., Correia, J.A.F.O., Susmel, L., Fernandes, A.A., May 2020. Low and ultra-low-cycle fatigue behavior of X52 piping steel based on theory of critical distances. Int. J. Fatig. 134, 105482. https://doi.org/10.1016/j.ijfatigue.2020.105482.

Peterson, R.E., Sines, G., Waisman, J.L., 1959. Notch sensitivity. In: Metal Fatigue. McGraw Hill, New York, pp. 293–306 [Online]. Available: https://ci.nii.ac.jp/naid/20001274434/. (Accessed 24 March 2021).

Refai, K., Brugger, C., Montemurro, M., Saintier, N., Sep. 2020. An experimental and numerical study of the high cycle multiaxial fatigue strength of titanium lattice structures produced by Selective Laser Melting (SLM). Int. J. Fatig. 138, 105623. https://doi.org/10.1016/j.ijfatigue.2020.105623.

Ronan, W., Deshpande, V.S., Fleck, N.A., Dec. 2016. The tensile ductility of cellular Solids: the role of imperfections. Int. J. Solid Struct. 102–103, 200–213. https://doi.org/10.1016/j.ijsolstr.2016.10.004.

Seiler, P.E., Li, K., Deshpande, V.S., Fleck, N.A., Dec. 2020. The influence of strut waviness on the tensile response of lattice materials. J. Appl. Mech. 88 https://doi.org/10.1115/1.4049140, 31011.

Simone, A.E., Gibson, L.J., Mar. 1998. Effects of solid distribution on the stiffness and strength of metallic foams. Acta Mater. 46 (6), 2139–2150. https://doi.org/10.1016/S1359-6454(97)00421-7.

Susmel, L., Taylor, D., Feb. 2010. An elasto-plastic reformulation of the theory of critical distances to estimate lifetime of notched components failing in the low/medium-cycle fatigue regime. J. Eng. Mater. Technol. 132 https://doi.org/10.1115/1.4000667, 21002.

Tankasala, H.C., Deshpande, V.S., Fleck, N.A., Dec. 2017. Tensile response of elastoplastic lattices at finite strain. J. Mech. Phys. Solid. 109, 307–330. https://doi.org/10.1016/j.jmps.2017.02.002.

Taylor, D., 2010. The Theory of Critical Distances: A New Perspective in Fracture Mechanics. Elsevier.

Tomažinčič, D., Nečemer, B., Vesenjak, M., Klemenc, J., 2019. Low-cycle fatigue life of thin-plate auxetic cellular structures made from aluminium alloy 7075-T651. Fatig. Fract. Eng. Mater. Struct. 42 (5), 1022–1036. https://doi.org/10.1111/ffe.12966.

Tomažinčič, D., Vesenjak, M., Klemenc, J., Apr. 2020. Prediction of static and low-cycle durability of porous cellular structures with positive and negative Poisson's ratios. Theor. Appl. Fract. Mech. 106, 102479. https://doi.org/10.1016/j.tafmec.2020.102479.

Wang, A.-J., McDowell, D.L., Apr. 2004. In-plane stiffness and yield strength of periodic metal honeycombs. J. Eng. Mater. Technol. 126 (2), 137–156. https://doi.org/10.1115/1.1646165.

Warren, W.E., Kraynik, A.M., Dec. 1997. Linear elastic behavior of a low-density kelvin foam with open cells. J. Appl. Mech. 64 (4), 787–794. https://doi.org/10.1115/1.2788983.

Yvonnet, J., 2019. Computational Homogenization of Heterogeneous Materials with Finite Elements. Springer International Publishing. https://doi.org/10.1007/978-3-030-18383-7.

Zhao, S., Li, S.J., Hou, W.T., Hao, Y.L., Yang, R., Misra, R.D.K., Jun. 2016. The influence of cell morphology on the compressive fatigue behavior of Ti-6Al-4V meshes fabricated by electron beam melting. Journal of the Mechanical Behavior of Biomedical Materials 59, 251–264. https://doi.org/10.1016/j.jmbbm.2016.01.034.

Zhu, H.X., Knott, J.F., Mills, N.J., Mar. 1997. Analysis of the elastic properties of open-cell foams with tetrakaidecahedral cells. J. Mech. Phys. Solid. 45 (3), 319–343. https://doi.org/10.1016/S0022-5096(96)00090-7.

Zhu, W., Blal, N., Cunsolo, S., Baillis, D., Jun. 2017. Micromechanical modeling of effective elastic properties of open-cell foam. Int. J. Solid Struct. 115–116, 61–72. https://doi.org/10.1016/j.ijsolstr.2017.02.031.

Zhu, S.-P., Liu, Y., Liu, Q., Yu, Z.-Y., Aug. 2018. Strain energy gradient-based LCF life prediction of turbine discs using critical distance concept. Int. J. Fatig. 113, 33–42. https://doi.org/10.1016/j.ijfatigue.2018.04.006.